High Frequency Focal Transducer with a Fresnel Zone Plate for Intravascular Ultrasound

Min Su[1,2,a)], Xiangxiang Xia[2,a)], Baoqiang Liu[2,3,a)],Zhiqiang Zhang[2], Rong Liu[2], Feiyan Cai[2], Weibao Qiu[2,4,b)], Lei Sun[1,b)]

[1]Department of Biomedical Engineering, The Hong Kong Polytechnic University, Hong Kong, China
[2]Paul C. Lauterbur Research Center for Biomedical Imaging, Shenzhen Institutes of Advanced Technology, ChineseAcademy of Sciences, Shenzhen, China
[3]Shenzhen College of Advanced Technology, University of Chinese Academy of Sciences, Shenzhen, China
[4]Shenzhen key laboratory of ultrasound imaging and therapy, Shenzhen, China

The diameter of an intravascular ultrasound (IVUS) catheter is always less than 1 mm because it must be inserted into a blood vessel to obtain ultrasound images. Owing to this requisite small size, it is difficult to perform geometric focusing on the surface of an IVUS transducer to improve the spatial resolution of the image. This study proposes a high frequency transducer with a Fresnel Zone Plate (FZP) for intravascular ultrasound imaging. Through theoretical calculations, the parameters and structure of the transducer are optimized for high-frequency ultrasound. The acoustic beam is simulated using COMSOL software. The aperture size of the ultrasound element is 0.778×0.9 mm^2. Transducers with or without the FZP layer are designed and fabricated in this study. The center frequency and -6 dB bandwidth of the FZP transducer are 52.5 MHz and 42%, respectively. Meanwhile, the center frequency and -6 dB bandwidth of the plane-shape transducer are 51.3 MHz and 58%, respectively. Wire phantom and porcine artery imaging experiments were performed to evaluate the performance of the designed transducers. The spatial resolution of the FZP transducer is 46.8 μm axially and 183.6 μm laterally, and the resolution of the plane-shape transducer is 44.3 μm axially and 313.5 μm laterally. The results demonstrate that the FZP transducer provides superior lateral imaging resolution for IVUS applications.

[a)] Contributions: M. Su, X. Xia and B. Liu have contributed equally to this work.

[b)] Author to whom correspondence should be addressed: wb.qiu@siat.ac.cn and lei.sun@polyu.edu.hk

Atherosclerotic plaque (AP) forms in the late stages of atherosclerosis. As the plaque accumulates, the associated gradual decrease in the area of the lumen leads to poor blood flow, which in turn, may further lead to myocardial ischemia and hypoxia[1,2]. Unstable and vulnerable plaques also may rupture instantaneously under certain circumstances, such as sudden strenuous exercise, and ruptured plaques can lead to catastrophic acute vascular events, such as myocardial infarction or sudden cardiac death[3]. The large lipid necrotic core (LNC) and thin-cap fibroatheroma (TCFA) are the main components of vulnerable plaques, and TCFA is usually less than 65μm in size[4]. Therefore, in order to reliably evaluate the extent of AP formation, it is expected that the imaging technique has excellent spatial resolution.

Computed tomography (CT) and magnetic resonance imaging (MRI) are advantageous diagnostic tools because they are non-invasive, but their poor spatial resolution impairs the corresponding assessment[5]. Meanwhile, optical coherence tomography (OCT) and intravascular ultrasound (IVUS) are minimally invasive diagnostic technology, where imaging catheters are inserted into blood vessels to acquire high-resolution images of AP. The spatial resolution of OCT is about 10μm, and as a result, OCT can be used to diagnose the presence of TCFA[6,7]. However, the penetration depth of OCT is short (1-2 mm)[8,9], and light attenuation in blood is huge[10], which limit the application of OCT. By comparison, IVUS has good resolution, can distinguish between different layers of arterial wall, and has a larger penetration depth, thus enabling the imaging of large plaques in real time[11]. As such, IVUS is not only an important diagnostic method for identifying vascular plaque, but also is a good guide for evaluating the location and suitability of postoperative stents[12]. However, traditional IVUS uses frequencies between 20 to 45 MHz which provide an axial resolution of 60–120 μm and a lateral resolution of 150–250 μm[13], and these frequencies do not meet resolution needs for detecting the presence of TCFA. While, it is reported that ultra-high frequency (> 80MHz) IVUS provides superior axial resolution (~ 20 μm)[14,15,16], the lateral resolution is still poor, and the penetration depth is limited as high-frequency ultrasound waves are highly attenuated. Chen et al. and Lee et al. proposed a focused IVUS transducer that would have better performance for intravascular imaging[17,18]. However, geometrically-focused IVUS transducers are difficult to fabricate because of their small sizes (<1 mm). Furthermore, to produce a well focused acoustic field, the piezoelectric elements need to be larger in size than traditional plane-shaped elements, which limits their clinical applications.

Acoustic meta-lenses have gradually become an important focusing technology for imaging applications. A low frequency (< 1MHz) single transducer with an acoustic lens can acquire better ultrasonic images than traditional plane-shape transducers[19]. However, meta-lenses are rarely used in high frequency transducers because the meta-lens layer significantly attenuates high frequency ultrasound waves. A Fresnel Zone Plate (FZP) is a thin zone-type lens based on the concept of Fresnel zones. It can be used to focus wave fields due to the diffraction characteristics of waves. There are two types of FZPs: Soret-type FZPs and phase-reversal FZPs[20,21,22]. A Soret-type FZP consists of alternating zones that are acoustically transparent and acoustically opaque to ensure the waves are diffracted from the transparent zones and focused to the focal point[20]. Soret-type FZPs are easily implement in

air[23,24] because solid materials (with high attenuation constants or high impedance contrasts with the host medium) and air can be regarded as acoustically opaque zones and

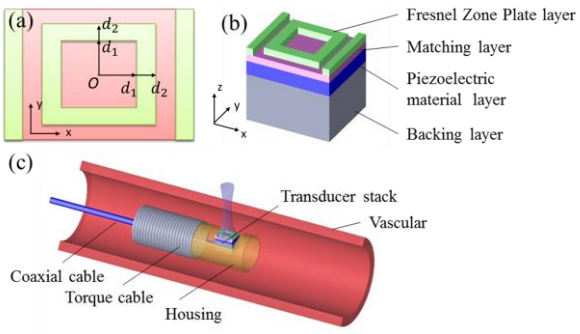

Fig. 1. (a) Illustration of the Fresnel Zone Plate. (b) The structure of the proposed transducer stack. (c) The proposed scheme of FZP IVUS

acoustically transparent zones, respectively. Different from Soret-type FZPs, phase-reversal FZPs replace acoustically opaque zones with phase-reversal zones that correct for the pressure contributions to the phase by adding a π phase change that generates constructive interference at the focal length. This phase change can be realized by changing the thickness or materials of the adjacent zones[21,22]. Thus, while both acoustically transparent zones and phase-reversal zones contribute to the focal region in a PR-FZP, only acoustically transparent zones contribute to the focal region in a Soret-type. Consequently, here a design for a PR-FZP transducer is proposed as it can improve both the lens efficiency and focal intensity[22]. By stacking a FZP onto the surface of a single plane transducer, the acoustic waves emitted from the proposed transducer will be diffracted by the Fresnel zones and converge into a focal region[25], in which the full width at half maximum (FWHM) of the field is smaller than that of a single plane transducer without a FZP. In other words, the incorporated FZP both increases the intensity and reduces the focal point size of a single transducer.

In this study, a high-frequency single element transducer containing a FZP layer is proposed for use in IVUS applications. The FZP layer is stacked on the surface of a high frequency single IVUS transducer to improve the imaging resolution of the IVUS, where diffraction of the waves through the Fresnel Zone causes the waves to converge at the focal region. The acoustic fields generated by the FZP transducer and plane-shaped transducer were simulated using finite element simulation software. The impedance and pulse echo of the transducers were characterized. These transducers were driven by a high frequency imaging system made in house, and wire phantom and porcine artery imaging

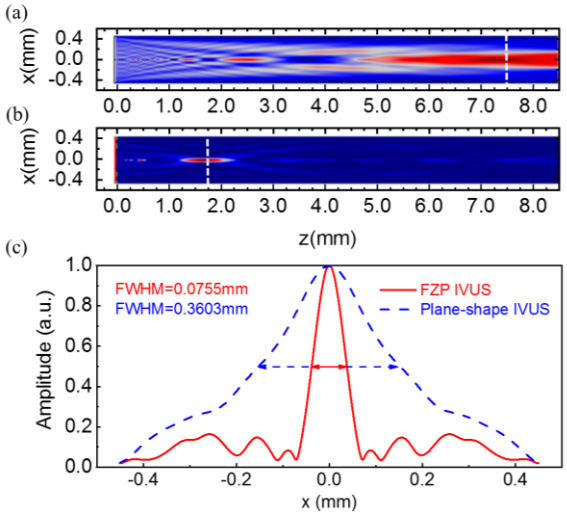

Fig. 2. (a) The acoustic field of the plane-shape IVUS. (b) The acoustic field of the FZP IVUS. (c) The amplitude distributions along the white dashed lines in the focal planes in the panels (a) and (b).

experiments were performed to verify the axial and lateral resolution of the proposed FZP and plane-shape transducers.

The designed structure of the proposed transducer is shown in Fig. 1. A FZP layer is deposited on front of the matching layer. The parameters of the FZP layer were calculated according to the Fresnel principle as follows.

In our work, the Fresnel zones of the FZP was calculated based on the equation for plane waves as

$$\boldsymbol{d_n = \sqrt{n\lambda F + (\frac{n\lambda}{2})^2}} \qquad (1)$$

where d_n (n = 1, 2, …, N) is the width of each zone from the center of the transducer, and N is the total number of Fresnel zones, and F = 2 mm is the focal length. The width of a FZP layer (shown as the green zones in Fig. 1) is $W_n = d_{2n}$-d_{2n-1}.

TABLE 1. Parameters of the FZP transducer and plane-shape transducer.

Parameter	FZP transducer	Plane-shape transducer
Aperture size (mm)	0.778×0.9	0.778×0.9
Piezo- material	PZT-5H	PZT-5H
Thickness (μm)	35	35
1st Matching layer material	Ag/epoxy	Ag/epoxy
Thickness (μm)	10	10
2st Matching layer material	N/A	Parylene C
Thickness (μm)	N/A	12
Fresnel Zone Plate layer material	Ag/epoxy	N/A
Thickness (μm)	8	N/A
Backing layer material	E-solder 3022	E-solder 3022
Thickness (μm)	300	300

To ensure the focusing effect of the incorporated FZP, there should be a π phase difference between the FZP layer and the consecutive groove (shown as the red zone =in Fig. 1(a)). The phase difference Δφ can be calculated by

$$\boldsymbol{\Delta\varphi = \frac{2\pi}{\lambda}\frac{|c_0 - c_1|}{c_1}\, t} \qquad (2)$$

where c_0 = 1500 m/s is the sound speed of water mand c_1 is the longitudinal sound speed in the FZP layer material, λ is the wavelength at the frequency in water, f is the frequency and t is the thickness of FZP layer.

In this work, the COMSOL simulation software (COMSOL Multiphysics 5.2a, Stockholm, Sweden) was used to calculate the acoustic field and optimize the structure and size of the proposed transducer. To reduce the computational costs, a 2D geometry was used in the simulations. Matching layers were used to avoid reflections at the external boundaries. The simulation parameters for the FZP transducer and plane-shape transducer are listed in Table I. The calculated acoustic fields of the transducers are shown in Fig. 2. As shown in Fig. 2(a), the natural focus of the plane-shape transducer is located at 7.5 mm, and a small focal spot with weak side-lobes was generated by the FZP transducer at a focal length of F = 1.8 mm (as shown in Fig. 2b). Figure 2(c) shows the amplitude distributions along the white dashed lines on the focal planes shown in Figs. 2(a) and 2(b). Clearly, the FWHM of the FZP IVUS (FWHM = 0.0755 mm) was smaller than that of the plane-shape IVUS (FWHM = 0.3603 mm), and the side-lobes were weaker in the FZP IVUS than in the IVUS. The simulated results shown in Fig. 2 demonstrate that the FZP layer can efficiently modulate the waves generated by the plane-shape IVUS, and the small FWHM of the amplitude calculated for the FZP IVUS illustrates that it has a higher lateral imaging resolution than the plane-shape IVUS.

PZT-5H (3203HD, CTS, Tianjing, China) was selected to fabricate the transducers for its high electromechanical coupling coefficient and performance stability. First, a Cr/Au electrode

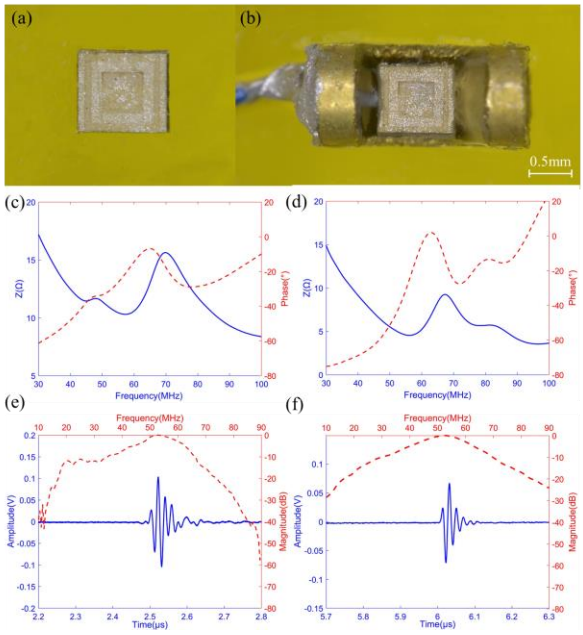

Fig.3. (a) Image of a representative piezo-stack. (b) The piezo-stack assembled in a copper housing. Measured impedance (blue solid line) and phase (red dotted line) of the FZP transducer (c) and plane-shape transducer (d). Measured echo (blue solid line) and spectrum (red dotted line) of the FZP transducer (e) and plane-shape transducer (f)

was sputtered on one side of the ceramic samples using a sputtering system (NSC-3500, NANO-MASTER, Inc., TX, USA). Next, this side of the sample was glued to the surface of a sapphire plate with wax, and the sapphire plate was placed on a lap machine. (EJ-380IN-D, Engis-Japan Co., Ltd., Yokohama, JAPAN) The ceramic samples were lapped to 35 μm, and then the other Cr/Au electrode was sputtered on the samples. Silver powder containing 2~3 μm particles in size (Sigma Aldrich, Burlington, USA) was mixed with epoxy (Insulcast 502, ITW Polymers Coatings North America, Montgomeryville, PA) and used to fabricate the matching layers and FZP layers because the mixture had a suitable acoustic impedance and conductivity. The mixture was deposited on the surface of ceramic samples, and the samples were then lapped to 18 μm, (for the plane-shape transducer, the thickness of this layer was 10 μm). Finally, the samples were turned over and conductive adhesive (E-Solder 3022, Von Roll USA Inc., Schenectady, NY, USA) was deposited on the back side of the samples to fabricate the backing layer. After the surface of the backing layer was ground, the sample was flipped back over and a laser machine (EP-IRPS-20, Han's Laser Technology Industry Group Co., Ltd, Shenzhen, China) was used to etch kerfs in the upper surface to shape the FZP layer. The depth of the kerfs was 8 μm. Then, the samples were diced into small piezo-stacks (0.778×0.9 mm^2) using a dicing saw (ADT 7022, Advanced Dicing Technologies, Israel). A representative image of a single piezo-stack is shown in Fig. 3(a). There were three steps to connect the positive and negative electrode leads to the transducers. First, the backing layer was connected to the signal wire in a coaxial cable with conductive adhesive. Second, the piezo-stacks were assembled into a copper housing (1.2 mm diameter, 2.5 mm length), and the housing and the ground wire of the coaxial cable were bound together. Finally, the space between the piezo-stack and the housing layer was filled with epoxy (Epo-Tek 301, Epoxy Technologies, Billerica, MA, USA) (as shown in Fig 3b), and the surface of the matching layer and copper housing were sputtered with a layer of Cr/Au to connect them together.

An impedance analyzer (WK 6500B, Wayne Kerr Electronics, Bognor Regis, UK) was used to measure the electrical impedance of the transducers. The transducers were immersed in a deionized water bath, and a quartz target with a polished surface was placed on front of the transducers to measure the pulse-echo response. The transducers were excited with a pulser/receiver (UT340, Utex Scientific Instruments Inc., Mississauga, Ontario, Canada). The pulse length was 2 ns, the applied voltage

was 100 V, and the echoes after amplification (10 dB gain) were recorded on a digital oscilloscope (DPO 4104, Tektronix Inc., Beaverton, OR, USA).

An imaging system that was specifically designed in house to evaluate IVUS imaging devices was used to drive the transducers[26]. The pulse was generated by two metal-oxide-semiconductor field effect transistor (MOSFET) pairs (TC6320, Supertex Inc., Sunnyvale, CA). Two drivers (EL7158, Intersil Corporation, Milpitas, CA) and a field programmable FPGA device (Cyclone-V 5CGXFC7D7F31C8N, Altera Corporation, San Jose, CA) were used to excite the MOSFETs. The programmable FPGA was used to control the excitation pulse parameters, such as the center frequency and number of pulse cycles. During data acquisition, the signal gain was set to 35 dB. The analog signals were digitized by a 12-bit ADC (AD9230, Analog Devices, Canton, MA) with a maximum sampling rate of 250 mega-samples per second (MSPS) before being transferred to an FPGA (Cyclone-V 5CGXFC7D7F31C8N, Altera Corporation, San Jose, CA) via a low-voltage differential signaling interface. High-speed signal processing was feasible for the FPGA, and a USB 3.0 interface (CYUSB3014, Cypress, San Jose, CA) was used to transfer the final ultrasound data to a computer.

Figs. 3(c) and (d) show the electrical impedance magnitude and phase measured for the FZP and plane-shape transducers, respectively. The measured resonance frequency of the FZP transducer was 57.3 MHz, and the impedance was 10.3 Ω at the resonance frequency. Meanwhile, the resonance frequency of the plane-shape transducer was 56.3 MHz, and the impedance was 4.5 Ω at the resonance frequency. The similar results for the two types of transducers show that the addition of the FZP layer had little effect on the electrical impedance of the transducer. The recorded pulse echo responses of the FZP and plane-shape transducers are illustrated in Figs. 3(e) and (f), respectively. The center frequencies of the FZP and plane-shape transducers were 52.5MHz and 51.3MHz, respectively, and the -6 dB bandwidths were 42% and 58%, respectively. As a result of the FZP layer and the lack of the second matching layer, the -6 dB bandwidth of FZP transducer was worse than that of plane-shape transducer.

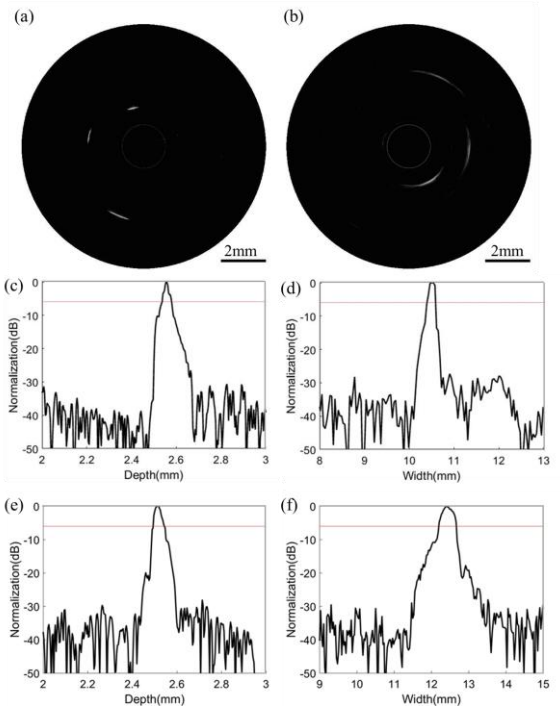

Fig. 4. Wire phantom ultrasonic images acquired with the FZP transducer (a) and the plane-shape transducer (b). Axial (c) and lateral (d) profile distances of the FZP transducer. Axial (e) and lateral (f) profile distances of the plane-shape transducer. The red lines in this figures show −6-dB magnitude.

Three 12.7 μm diameter tungsten wires (California Fine Wire Company, Grover Beach, CA) were placed on concentric circles with

different radii (2 mm, 3 mm, and 4 mm) to fabricate a wire phantom and evaluate the imaging resolution of the different transducers. During the imaging process, the transducers and wire phantom were placed in a container with deionized water, and the transducers were held in the center of the wire phantom. The transducers were connected to the ultrasound imaging system and rotated with a tiny motor. After the imaging process, the ultrasound system collected the image data. Then, the

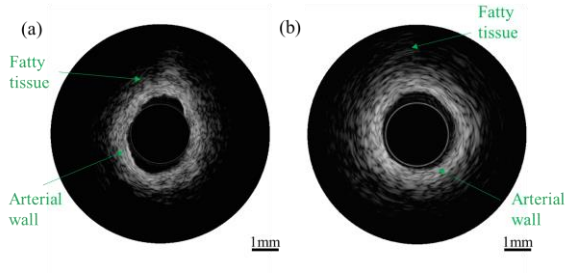

Fig. 5. Images of a porcine artery taken with the (a) FZP transducer and (b) plane-shape transducer. image.

Matlab software suite was (MathWorks Inc., Natick, MA) used to plot the wire phantom images and calculate the imaging resolution. Fig. 4(a) and (b) show the ultrasonic images acquired with the FZP and plane-shape transducers, respectively. Fig. 4 (c-f) shows the axial and lateral beam profiles. The axial and lateral resolution of the FZP transducer were 46.8 μm and 183.6 μm, respectively. The axial and lateral resolution of the plane-shape transducer were 44.3 μm and 313.5 μm, respectively. It can be seen that the lateral resolution of the FZP transducer was better than that of the plane-shape transducer. The SNRs (signal to noise) were calculated by subtracting the average noise floor from the maximum amplitude and were found to be 37.2 dB and 33.9 dB for the FZP and plane-shape transducer, respectively. The higher SNR of the FZP transducer confirms it shows better imaging performance. The ultrasonic images of a piece of porcine artery were also obtained with the FZP and plane-shape transducers, as shown in Fig. 5, and the arterial wall and fatty tissue were more clearly distinguishable in the image acquired with the FZP transducer than the in image taken with the plane-shape transducer.

IVUS imaging is an important detection technology for atherosclerotic plaque; however, the poor lateral resolution of current IVUS catheters limits their application. Here, a high frequency transducer with an FZP was proposed to improve the lateral resolution of IVUS imaging. The diameter of the proposed transducer (1.2 mm) is larger than that of commercial transducers, but it can be reduced by sophisticated manufacturing of its housing. The center frequency of the designed transducer was 52.5 MHz. The acoustic beam of the proposed transducer containing the FZP and a plane-shape transducer with the equivalent size were simulated in COMSOL. The size of focal zone was significantly reduced in the proposed transducer containing the FZP layer. The electrical impedance (~10 Ω) of the proposed transducer mismatch the imaging system (50 Ω), resulting in a weaker echoic signal amplitude. To solve the problem, a more suitable piezoelectric material with lower dielectric constant will be chosen to fabricate FZP transducer in the future. The -6dB bandwidth of the FZP transducer (42%) was worse than that of plane-shape transducer (58%) because of the influence of FZP layer and lack of a second matching layer. The poorer performance may have due to the weaker bandwidth, and the axial resolution of the FZP transducer (46.8 μm) was worse than plane-shape transducer (44.3μm). Meanwhile, wire phantom images and resolution beam profiles showed that the lateral resolution of the FZP transducer was

significantly improved. Because of the similar acoustic impedance of arterial wall and fatty tissue, it is not easy to distinguish them from the original ultrasound image. Nevertheless, the FZP transducer presented a better resolution in ex vivo imaging of a porcine artery.

ACKNOWLEDGEMENTS

This research was funded by the National Natural Science Foundation of China (12004411, 62022086, 11874382, 11804358, and 12004408), Youth Innovation Promotion Association CAS 2018391, CAS research projects (QYZDB-SSW-JSC018, GJJSTD20180002, and 2011DP173015), Shenzhen Foundation Grant (JCYJ20170817171836611, JCYJ20180302145531853, JCYJ20190806171405522, and ZDSYS201802061806314), National Basic Research Program of China (2019YFC0121100), Guangdong Special Support Program, and Natural Science Foundation of Guangdong Province (2020B1212060051 and 2020B1111130002)

NO CONFLICTS OF INTEREST

The authors have no conflicts to disclose.

DATA AVAILABILITY

The data that support the findings of this study are available upon reasonable request from the corresponding authors.

REFERENCES

[1]R. Virmani, F. D. Kolodgie, A. P. Burke, A. Farb, and S. M. Schwartz, Arterioscl Throm Vas **20** (5), 1262 (2000).

[2]John A Ambrose and Amarbir S Bhullar, EMJ **4** (1), 71 (2019).

[3]F. Otsuka, M. C. A. Kramer, P. Woudstra, K. Yahagi, E. Ladich, A. V. Finn, R. J. de Winter, F. D. Kolodgie, T. N. Wight, H. R. Davis, M. Joner, and R. Virmani, Atherosclerosis **241** (2), 772 (2015).

[4]R. Virmani, A. P. Burke, A. Farb, and F. D. Kolodgie, Journal of the American College of Cardiology **47** (8 Suppl), C13 (2006).

[5]D. R. Obaid, P. A. Calvert, D. Gopalan, R. A. Parker, S. P. Hoole, N. E. J. West, M. Goddard, J. H. F. Rudd, and M. R. Bennett, Circ-Cardiovasc Imag **6** (5), 655 (2013).

[6]B. Povazay, K. Bizheva, A. Unterhuber, B. Hermann, H. Sattmann, A. F. Fercher, W. Drexler, A. Apolonski, W. J. Wadsworth, J. C. Knight, P. S. J. Russell, M. Vetterlein, and E. Scherzer, Opt Lett **27** (20), 1800 (2002).

[7]M. J. Suter, S. K. Nadkarni, G. Weisz, A. Tanaka, F. A. Jaffer, B. E. Bouma, and G. J. Tearney, Jacc-Cardiovasc Imag **4** (9), 1022 (2011).

[8]M. Kawasaki, B. E. Bouma, J. Bressner, S. L. Houser, S. K. Nadkarni, B. D. MacNeill, I. K. Jang, H. Fujiwara, and G. J. Tearney, Journal of the American College of Cardiology **48** (1), 81 (2006).

[9]T. Kubo, T. Akasaka, J. Shite, T. Suzuki, S. Uemura, B. Yu, K. Kozuma, H. Kitabata, T. Shinke, M. Habara, Y. Saito, J. B. Hou, N. Suzuki, and S. S. Zhang, Jacc-Cardiovasc Imag **6** (10), 1095 (2013).

[10]B. D. MacNeill, H. C. Lowe, M. Takano, V. Fuster, and I. K. Jang, Arterioscl Throm Vas **23** (8), 1333 (2003).

[11]N. W. Shammas, Q. Radaideh, W. J. Shammas, G. E. Daher, R. J. Rachwan, and Y. Radaideh, Vascular health and risk management **15**, 283 (2019).

[12]C. di Mario, K. C. Koskinas, and L. Raber, Journal of the American College of Cardiology **72** (24), 3138 (2018).

[13]F. S. Foster, C. J. Pavlin, K. A. Harasiewicz, D. A. Christopher, and D. H. Turnbull, Ultrasound In Medicine And Biology **26** (1), 1 (2000).

[14]C. E. Munding, E. Cherin, N. Alves, D. E. Goertz, B. K. Courtney, and F. S. Foster, Ultrasound In Medicine And Biology **46** (8), 2104 (2020).

[15]M. Su, Z. Zhang, J. Hong, Y. Huang, P. Mu, Y. Yu, R. Liu, S. Liang, H. Zheng, and W. Qiu, IEEE Trans Ultrason Ferroelectr Freq Control **66** (5), 849 (2019).

[16]T. Ma, M. Yu, J. Li, C. E. Munding, Z. Chen, C. Fei, K. K. Shung, and Q. Zhou, IEEE Trans Ultrason Ferroelectr Freq Control **62** (1), 97 (2015).

[17]Y. Chen, W. B. Qiu, K. H. Lam, B. Q. Liu, X. P. Jiang, H. R. Zheng, H. S. Luo, H. L. W. Chan, and J. Y. Dai, Ultrasonics **56**, 227 (2015).

[18]J. Lee, J. Jang, and J. H. Chang, Ieee T Bio-Med Eng **64** (3), 671 (2017).

[19]Y. X. Shen, Y. G. Peng, F. Y. Cai, K. Huang, D. G. Zhao, C. W. Qiu, H. R. Zheng, and X. F. Zhu, Nat Commun **10** (2019).

[20]D. C. Calvo, A. L. Thangawng, M. Nicholas, and C. N. Layman, Applied Physics Letters **107** (1) (2015).

[21]X. X. Xia, Y. C. Li, F. Y. Cai, H. Zhou, T. Ma, and H. R. Zheng, Applied Physics Letters **117** (2) (2020).

[22]D. Tarrazo-Serrano, S. Perez-Lopez, P. Candelas, A. Uris, and C. Rubio, Scientific reports **9** (2019).

[23]John T Welter, Shamachary Sathish, Josiah M Dierken, Philip G Brodrick, Matthew R Cherry, and Jason D Heebl, Applied Physics Letters **100** (21), 214102 (2012).

[24]Miguel Molerón, Marc Serra-Garcia, and Chiara Daraio, Applied Physics Letters **105** (11), 114109 (2014).

[25]R. Lirette, J. Mobley, and L. K. Zhang, Phys Rev Appl **12** (6) (2019).

[26]W. Qiu, X. Wang, Y. Chen, Q. Fu, M. Su, L. Zhang, J. Xia, J. Dai, Y. Zhang, and H. Zheng, IEEE Trans Biomed Eng **64** (8), 1935 (2017).